JACS
JOURNAL OF THE AMERICAN CHEMICAL SOCIETY
Article
pubs.acs.org/JACS

Synthesis Design and Structure of a Multipore Zeolite with Interconnected 12- and 10-MR Channels

Manuel Moliner,[†] Tom Willhammar,[‡] Wei Wan,[‡] Jorge González,[†,§] Fernando Rey,[†] Jose L. Jorda,[†] Xiaodong Zou,*[,‡] and Avelino Corma*[,†]

[†]Instituto de Tecnología Química (UPV-CSIC), Universidad Politécnica de Valencia-Consejo Superior de Investigaciones Científicas, Av. De los Naranjos s/n, 46022 Valencia, Spain

[‡]Berzelii Centre EXSELENT on Porous Materials and Inorganic and Structural Chemistry, Department of Materials and Environmental Chemistry, Stockholm University, SE-106 91 Stockholm, Sweden

[§]Escuela de Ciencias Químicas, Universidad de Colima, Colima 28040, Mexico

Supporting Information

ABSTRACT: A new molecular sieve, ITQ-38, containing interconnected large and medium pores in its structure has been synthesized. The rational combination of dicationic piperidine-derivative molecules as organic structure directing agents (OSDAs) with germanium and boron atoms in alkaline media has allowed the synthesis of ITQ-38 zeolite. High-resolution transmission electron microscopy (HRTEM) has been used to elucidate the framework topology of ITQ-38, revealing the presence of domains of perfect ITQ-38 crystals as well as very small areas containing nanosized ITQ-38/ITQ-22 intergrowths. The structure of ITQ-38 is highly related to ITQ-22 and the recently described polymorph C of ITQ-39 zeolite. It shares a common building layer with ITQ-22 and contains the same building unit as the polymorph C of ITQ-39. All three structures present similar framework density, 16.1 T atoms/1000 Å^3.

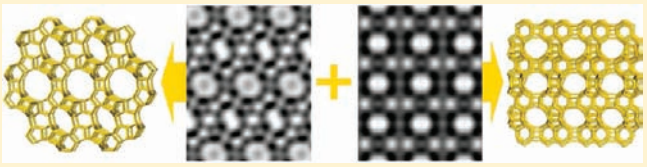

1. INTRODUCTION

Despite the large number of reported zeolites,[1] the discovery of a new material with unique structural characteristics, such as pore shape, size and channel dimensionality, is always attractive because of potential new and/or improved applications.[2] Zeolites are widely used as catalysts, and probably one of their most stunning features is their capability to induce different product selectivities depending on the pore topology.[3] In this sense, preparation of new zeolites with intersecting channels of different sizes allows the selective diffusion of reactants with different dimensions, with potential unique molecular transport through the zeolite, and inducing more favorable orientations to react and give the desired product.[4]

Important advances have been achieved in the synthesis of structures with intersecting extra-large and large,[5] extra-large and medium,[6] and specially, large and medium[7] pores. This last type of zeolites can also be of potential practical interest because they can combine in the same solid the pore topologies of medium and large pores.

Recently, we have reported the synthesis of a new complex structure, ITQ-39 zeolite family, which is formed by an intergrowth of three different polymorphs, all of them containing three-dimensional intersecting pairwise 12-membered rings (MR) and 10-MR pore systems.[8] ITQ-39 has been synthesized as an aluminosilicate using large dicationic piperidine derivatives as organic structure directing agent (OSDA) (see OSDA2 in Figure 1). Those type of organic molecules show a dramatic phase directing effect when their size and shape are tailored by introducing methyl, ethyl or propyl chains.[9] Indeed, ITQ-39 can be synthesized in a broader Si/Al ratio when the used OSDA is ethyl-substituted, avoiding in such case the crystallization of the competing ZSM-5 phase.[9]

One of the polymorphs in the ITQ-39 family, the polymorph C (ITQ-39C), contains double four-membered rings (D4Rs) in its structure,[8] but is only present in 10% enrichment in the ITQ-39 intergrowth. The directing effect of Ge toward zeolites containing D4Rs in their structures is well-known.[10] Indeed, the proposed theoretical structures for polymorph C of Beta zeolite family[11] and polymorph C of CON family,[12] both containing D4R in their frameworks, were first synthesized as pure phases when Ge was introduced, together with Si, in the gel preparation (ITQ-17 or FOS-5, and ITQ-24, respectively).[13]

Here, we will show a complete and rational experimental study with the main objective to direct the synthesis of ITQ-39C zeolite or other related zeolites containing large and medium pores having D4Rs in their structures. As will be described, a new zeolite, ITQ-38, has been discovered, which is closely related to the polymorph C of ITQ-39. Both contain similar framework density (16.1 T atoms/1000 Å^3), and are built from the same building unit. ITQ-38 is also related to ITQ-22 zeolite; both show the same building layer which is connected in different way. The discovery of ITQ-38 and its structural elucidation further confirm the excellent directing

Received: February 2, 2012
Published: March 22, 2012

   dx.doi.org/10.1021/ja301082n | J. Am. Chem. Soc. 2012, 134, 6473−6478

effect of dicationic piperidine molecules toward zeolites with interconnected large and medium pore zeolites when working in the appropriate synthesis conditions.

2. EXPERIMENTAL SECTION

2.1. Synthesis of the Organic Structure Directing Agents (OSDAs). The synthesis of OSDA2 has been previously described.[9] OSDA1, 1,1-dimethyl-4-(1-methylpirrolidine-1-yl)piperidinium, was prepared as follows: 10 g of pyrrolidine (Sigma-Aldrich, 99%) was dissolved in 100 mL of ethanol (Sigma-Aldrich, >99%). The solution was acidified with HCl (Fluka, 5 N in methanol) until pH = 7.5, cooling down the mixture continuously at 273 K. Then, 10 g of 1-methyl-4-piperidone (Sigma-Aldrich, 99%) was added, followed by 3.5 g of sodium cyanoborohydride ($NaBH_3CN$, Fluka, >95%). The resultant mixture was stirred during 72 h at room temperature.

Next, HCl was added slowly until pH was close to 2, with the HCN removed by nitrogen flow. The resulting solution was concentrated, and then, a KOH solution was added until pH > 12. The mixture was saturated with NaCl. Finally, the diamine 1-methyl-4-pyrrolidin-1-yl-piperidine (MPP) was extracted with diethyl ether and dried with anhydrous $MgSO_4$.

A total of 10.4 g of MPP was dissolved in 80 mL of MeOH, and then, 42 g of methyl iodide was added. After 7 days under stirring at room temperature, a white precipitate was achieved, which was filtered and washed with methanol and diethyl ether. Finally, the solid was dried under high vacuum. The iodide salt was converted to the hydroxide salt by treatment with a hydroxide anion exchange resin. The structure of the different OSDA is shown in Figure 1.

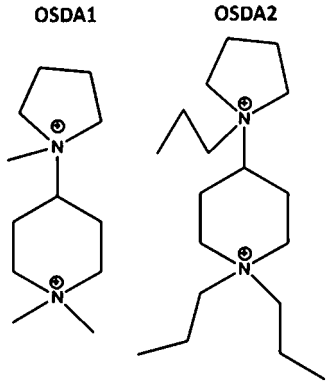

Figure 1. Organic structure directing agents (OSDAs) used in this work.

2.2. Zeolite Synthesis. In a typical zeolite synthesis procedure, boric acid (99.5%, Aldrich) or alumina (74.6%, Condea) and germanium oxide (99%, Aldrich) were dissolved in the OSDA hydroxide solution. Colloidal silica (Ludox AS-40, Aldrich) was added, followed by NH_4F (98%, Aldrich) if necessary. The gels were allowed to reach the desired water ratio by evaporation and, then, transferred to a Teflon lined stainless autoclaves and heated at 175 °C during 14 days. The solids were recovered by filtration, extensively washed with distilled water, and dried at 90 °C overnight.

2.3. Characterization. X-ray powder diffraction (XRPD) data were collected using a Panalytical X'Pert PRO diffractometer with Bragg–Brentano geometry, using Cu K_α radiation (λ_1 = 1.5406 Å, λ_2 = 1.5441 Å, I_2/I_1 = 0.5; divergence slit, fixed = 1/16°; goniometer arm length, 240 mm; detector, Panalytical X'Celerator; tube voltage and intensity, 45 kV, 40 mA; scan range, 3.0° to 75.0° (2θ); scan step size, 0.017° (2θ); counting time, 2400 s/step). Prior to the measurement of the calcined material, the sample was calcined in situ at 823K for 5 h under a continuous flow of dry air in an Anton Parr XRK-900 reaction chamber attached to the diffractometer, and allowed to be cooled again at room temperature.

High-resolution powder diffraction data for crystalline ITQ-38 were collected at Beamline BM01B at ESRF (λ = 0.5198 Å), using a calcined sample placed in a sealed glass capillary.

The chemical analysis was performed in a Varian 715-ES ICP-OES instrument, after dissolution of the solid in a HNO_3/HCl/HF aqueous solution. The organic content of the as-made materials was determined by elemental analysis performed on a SCHN FISONS elemental analyzer. Thermogravimetrical analysis was performed using a Mettler Toledo thermobalance.

The morphology of the samples was studied by scanning electron microscopy (SEM) using a JEOL JSM-6300 microscope.

Textural properties were determined by Ar and N_2 adsorption–desorption isotherms measured at 87 and 77 K, respectively, with a Micromeritics ASAP 2020.

Transmission electron microscopy (TEM) was used for solving the structure of ITQ-38 and studying the intergrowth of ITQ-22 and ITQ-38. TEM samples of as-synthesized ITQ-38 were either prepared directly from the powder or cut by ultramicrotomy. High-resolution transmission electron microscopy (HRTEM) was performed on a JEOL JEM-2100F microscope equipped with a field emission gun operated at an accelerating voltage of 200 kV (point resolution 1.9 Å). The images were recorded on a Gatan Ultrascan 1000 2k × 2k CCD camera. Because ITQ-38 was very electron beam sensitive, low dose conditions were applied and a through-focus series of 20 HRTEM images with a constant focus step of 106.6 Å was recorded using a DigitalMicrograph script.[14] The defocus and astigmatism for each image were determined and the structure projection was reconstructed by combining the corrected HRTEM images to enhance the signal-to-noise level, using the program *QFocus*, which is an implementation of the structure projection reconstruction method.[15] Selected area electron diffraction (SAED) was recorded on a JEOL JEM-2100 microscope. Simulation of electron diffraction patterns was done using the program CrystDiffract,[16] taking into account the effects of Ewald sphere and the excitation errors using a thickness of 12 nm.

Projected potential maps were obtained by crystallographic image processing using the software CRISP.[17] Structure factor amplitudes and phases were extracted from the lattice points in the Fourier transform of each image, from which the projection symmetry was determined. The atomic coordinates in the projection were obtained from the map after imposing the projection symmetry.

3. RESULTS AND DISCUSSION

3.1. Synthesis. As it has been described above, germanium shows a remarkable directing effect toward zeolites containing D4R units.[10] This fact is explained because the Ge–O–Si angles are smaller than those of Si–O–Si, stabilizing the D4R cages when Ge atoms are present.[18] Also, a similar directing effect has been observed when syntheses are carried out in the presence of fluoride anions.[19] In this case, it has been observed that fluoride ions are preferentially located inside of D4R units, stabilizing those small cages by formation of five-coordinated $SiO_{4/2}F^-$ units.[20] Following those two premises, we designed two sets of exploratory experimental designs for synthesis of new porous materials in presence of Ge and fluoride anions (see Table S1 in Supporting Information). Synthesis variables such as germanium, boron, aluminum, and gel concentration were investigated using dicationic piperidine derivatives OSDA1 and OSDA2. A total of 30 experiments were performed, achieving the two phase diagrams summarized in Figure S1 in Supporting Information. As it can be seen, BEC zeolite is formed in the presence of high Ge contents in the synthesis gel for both OSDAs. This is not surprising, since BEC has often been described as one of the most stable structures in Ge-rich gels with a large variety of OSDAs.[13a] However, the phase selectivity is very different depending on the size and flexibility of the used OSDA when working at higher Si/Ge ratios. The medium-sized OSDA1 directs to the formation of

dx.doi.org/10.1021/ja301082n | J. Am. Chem. Soc. 2012, 134, 6473–6478

the clathrate octadecasil (AST), which structure is also rich in D4Rs, while the large and flexible OSDA2 directs toward the formation of ZSM-5 (MFI) structure. This outcome has been rationalized by the similar flexibility of OSDA2 and TPA, which is the preferred OSDA for MFI synthesis.[9]

From those previous findings, we can conclude that three very stable phases (BEC, AST, and MFI) are formed in most of the explored areas, when syntheses are carried out in fluoride media. However, the fact that AST clathrate is obtained in a wide range of reaction conditions when OSDA1 is used as template reveals the higher directing effect of Ge and F than the organic molecule, since three-quarters of the total T-sites in AST clathrate are located at D4R units. Taking into account all the above observations, it appears that a different strategy must be applied in order to obtain open structures and, most importantly, to change significantly the phase selectivity toward structures other than the very stable BEC, AST and MFI.

Recently, the remarkable impact of the mobilizing agent (hydroxide or fluoride anions) in zeolite synthesis on phase selectivity has been reviewed by Zones et al.[21] They describe that materials with open structures (low framework densities) can be achieved in alkaline media in the presence of high aluminum or boron content under diluted conditions.[22] Then, following that premise, we decided to move toward alkaline media in order to study the phase selectivity of OSDA1 and OSDA2. The experimental design for the study in alkaline media is described in Table S2 in Supporting Information, where a total of 48 new experiments for both OSDAs are summarized. As seen in Figure S2, different phases are achieved in alkaline media than in fluoride media. OSDA2 directs the formation of Beta or MFI depending on the gel dilution, while OSDA1 directs the crystallization of BEC, AST, and mixtures of them in several synthesis conditions. However, in diluted concentrations (H_2O/T^{IV} = 10), a different unknown phase is also obtained as a mixture of phases together with BEC and AST. This new material is named ITQ-38.

ITQ-38 appears preferably at the highest gel dilution and using a Si/Ge ratio of 5. Consequently, a new set of conditions was defined for optimizing the preparation of ITQ-38, which involved two H_2O/T^{IV} ratios, three Si/Ge values, and different aluminum and boron contents, yielding an experimental design with 24 experiments (see Table S3). As seen in Figure S3, pure ITQ-38 was achieved in the presence of boron, Si/Ge ratios of 5 and 10, and high dilution conditions (H_2O/T^{IV} = 20). However, the samples are not fully crystalline, but also contain an amorphous phase. Taking into account that the sample with Si/Ge ratio of 5 shows less amorphous content than sample with Si/Ge ratio of 10, a new synthesis was undertaken where the Si/Ge ratio was decreased while keeping the dilution constant in order to reach the crystalline ITQ-38. The selected conditions were: Si/Ge = 3, H_2O/T^{IV} = 20, B/T^{IV} = 0.02, $OSDA1/T^{IV}$ = 0.25, at 175 °C. After 14 days, a fully crystalline ITQ-38 zeolite was achieved.

3.2. Characterization and Structure Solution. XRPD patterns of the as-prepared ITQ-38 sample and sample calcined at 550 °C indicate that the structure remains stable after the removal of the organic moiety (Figure S4 in Supporting Information). Elemental analyses of the as-prepared ITQ-38 reveal that the organic cation OSDA1 remains intact inside the ITQ-38 structure, showing a C/N molar ratio of 6.1, while thermogravimetric analyses give a weight loss of 15 wt % (see Figure S5).

To know the textural properties of ITQ-38, N_2 and Ar adsorption measurements were performed. The N_2 adsorption isotherm at 77 K shown in Figure S6 reveals the microporous nature of this material. The BET (Brunauer–Emmett–Teller) surface area is 367 m^2/g with a micropore volume of 0.16 cm^3/g. High-resolution Ar adsorption isotherm at 87 K enables us to obtain an accurate experimental pore distribution by applying the Howarth-Kamazoe formalism. As seen in Figure S7, a bimodal narrow pore distribution centered at 5.5 and 6.6 Å is observed, indicating that the ITQ-38 may present a large and medium pore channel system in its structure. The relative high adsorption capacity also suggests that this zeolite may be formed by a tridirectional system of pores.

Additionally, scanning electron microscopy (SEM) images (see Figure S8) show very small crystallites (0.1–0.2 μm). This crystal size precludes the solution by single-crystal X-ray diffraction.

Then, the structural elucidation of the ITQ-38 zeolite has been attempted from high-resolution X-ray powder diffraction (HR-XRPD) data collected using synchrotron radiation (see XRPD pattern in Figure S9). The XRPD pattern was successfully indexed in a monoclinic unit cell (a = 13.02 Å, b = 12.70 Å, c = 21.25 Å, β = 96.87°, V = 3489 $Å^3$) using the program TREOR.[23] The study of the systematic extinctions suggests as possible space groups $P2$, Pm or $P2/m$. However, the large peak overlapping even at very low 2θ angles due to the large unit cell and, as observed later, the presence of stacking faults in the crystals, precluded the structure solution from XRPD data by direct methods. Consequently, TEM was applied to solve the framework topology of ITQ-38.

SAED patterns taken along the three main axes confirmed the unit cell parameters of ITQ-38, as shown in Figure S10a–c in Supporting Information. HRTEM images of ITQ-38 (Figure 2a,d) show that ITQ-38 contains domains of perfect single crystals that give sharp spots (Figure 2b), as well as small areas

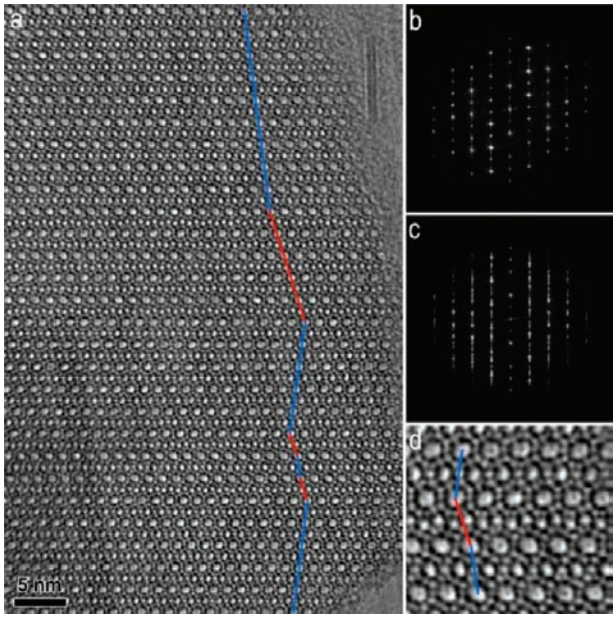

Figure 2. (a) Reconstructed structure projection along [010] of ITQ-38, showing the intergrowth of ITQ-38 (traced by blue lines, with 10- and 12-ring) with ITQ-22 (traced by red lines, with 8- and 12-rings) in the ab-plane of ITQ-38. (b and c) Fourier transforms from the region, (b) without and (c) with stacking faults. (d) Enlarged view of panel a.

dx.doi.org/10.1021/ja301082n | J. Am. Chem. Soc. 2012, 134, 6473–6478

with intergrown crystals that give streaks in the Fourier transforms (Figure 2c). The presence of those nanosized intergrown domains makes the structure resolution of ITQ-38 not achievable using only X-ray powder diffraction data. Thus, SAED and HRTEM combined with crystallographic image processing were used for structure solution. One of the important advantages of using HRTEM images is that the crystallographic structure factor phases, which are required for structure solution but are lost in diffraction, can be directly obtained from images.[24] Following this methodology, very complex structures have been solved during the last years.[10d,25]

The reconstructed HRTEM image along the [010] direction of ITQ-38 indicates that this material contains 10- and 12-rings along [010] (Figure 2d). In addition, regions with 8- and 12-rings are found (traced by red lines), which are identified as ITQ-22 (IWW),[7d] as shown in Figure 2a,d. Regions of ITQ-38 and ITQ-22 are stacked along the c*-axis of ITQ-38 (a*-axis of ITQ-22) with perfect match of the structures. ITQ-38 is significantly dominating, and crystals of pure ITQ-38 without the intergrowth were also found.

Crystallographic image processing was applied to the thin and defect-free regions of ITQ-38 in the reconstructed structure projection images along [010] and [101] using the software CRISP.[17] Structure factor amplitudes and phases were extracted from the lattice points in the Fourier transform of each image, from which the projection symmetry was determined to be *p*2 for the [010] projection (Figure 3a,

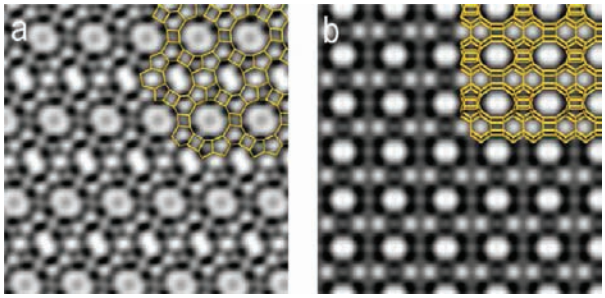

Figure 3. Projected potential map obtained by crystallographic image processing from defect-free regions along (a) [010] and (b) [101]. The structure model is superimposed for comparison.

average phase error for the structure factor phases extracted from the reconstructed HRTEM image about 8°) and *p*2*mm* along [101] projection (Figure 3b, average phase error ≈9°). Among the three possible space group *P*2, *Pm* or *P*2/*m*, only *P*2/*m* gives both the projection symmetry *p*2 along [010] and the projection symmetry *p*2*mm* along [101]. This indicates that the space group of ITQ-38 is *P*2/*m*.

The reconstructed projected potential map along the [010] projection in Figure 3a shows clearly that the structure of ITQ-38 contains 4-, 5-, 6-, 10- and 12-rings along [010]. The 10- and 12-rings alternate along c*. The layers containing the 12-rings are similar to those in ITQ-22 (see Figure 2a,d). However, they are connected in different ways along the c*-axis, forming alternating 6- and 10-rings in ITQ-38 and 8-rings in ITQ-22. In addition, as ITQ-38 has a *b* parameter (12.70 Å) similar to ITQ-22 (12.99 Å), a structure model of ITQ-38 could be deduced using the structure of ITQ-22 as a starting point, as shown in Figure 4a,c.

The structure model contains 16 symmetry-independent T-atoms (T = Si, Ge), and all are tetrahedrally coordinated to the

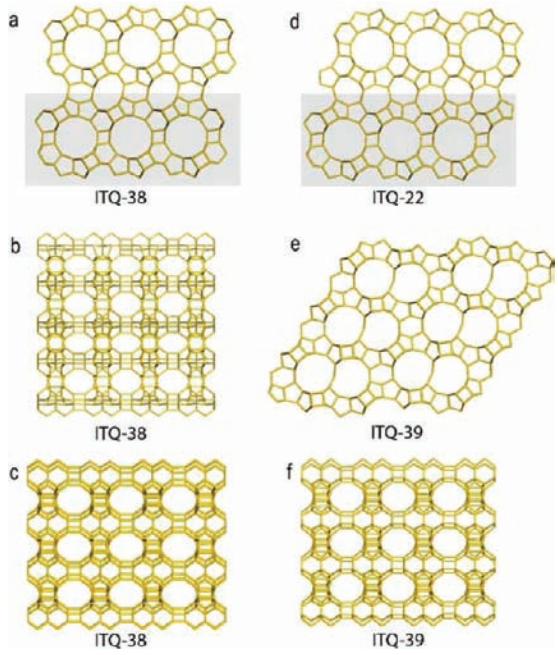

Figure 4. The structure model of ITQ-38 viewed along (a) [010], (b) [100], and (c) [101] directions; (d) ITQ-22 viewed along [001]; and ITQ-39C viewed along (e) [010] and (f) [100] directions. ITQ-38 contains 10- and 12-ring channels along [010] and 10-ring channels along [101] and [100]. ITQ-22 contains 8- and 12-ring channels along [001] and 10-ring channels along [010] and [120]. ITQ-39 contains pairwise 12-rings along [010] and 10-rings along [100].

framework oxygen atoms. The three-dimensional framework of ITQ-38 contains straight 10- and 12-ring channels along [010], and zigzag 10-ring channels along [100] and [101]. The structure was refined geometrically with a distance least-squares refinement, obtaining a RDLS value of 0.0027. The unit cell parameters of the refined structure model are a = 12.8726 Å, b = 12.8480 Å, c = 21.2200 Å, β = 96.23°, V = 3488.78 Å^3, in good agreement with those previously obtained from XRPD data, and also related to that described for ITQ-22 (a = 42.1326(1) Å, b = 12.9885(3) Å, c = 12.6814(2) Å, V = 6940 Å^3) but with only one-half of its volume. HRTEM images along the [101] projection further confirm the structure model (Figure 3b). Kinematic electron diffraction patterns calculated from the model match well with the experimental ones (Figure S10), which also confirms the model. The resulting atomic coordinates for ITQ-38 are shown in Table S4 in the Supporting Information.

To know whether the determined structure was representative of the entire sample, the unit cell parameters and symmetry of zeolite ITQ-38 were confirmed by a LeBail refinement of the experimental XRPD pattern collected using a laboratory diffractometer. The final refined cell parameters obtained using the program FullProf[26] were a = 12.921 Å, b = 12.939 Å, c = 21.348 Å, β = 96.80° and V = 3544.0 Å^3. The presence of stacking faults combined with the large complexity of the unit cell precluded a satisfactory Rietveld refinement of the full structure. In this sense, attempts to minimize the differences between the observed and calculated XRPD of ITQ-38 produced artificial and severe displacements of oxygen atoms out of the physically reasonable positions. Therefore, we proceeded to simulate the theoretical XRPD pattern of the proposed structure of ITQ-38 for visual comparison with the

dx.doi.org/10.1021/ja301082n | J. Am. Chem. Soc. 2012, 134, 6473−6478

experimental data, using the program FullProf. The background and profile parameters extracted from the LeBail refinement of the experimental data were used for this simulation. Taking into account the similarity between the layers of the intergrowth members (ITQ-22 and ITQ-38), we used the experimental values obtained for a sample of ITQ-22 with similar Si/Ge ratio (Si/Ge = 4)[26] to obtain an estimation of the Ge distribution in the different T sites of the ITQ-38 structure. Both experimental and simulated XRPD patterns are in good agreement, as shown in Figure 5. This confirms that the proposed ITQ-38 structure is the main component of the material.

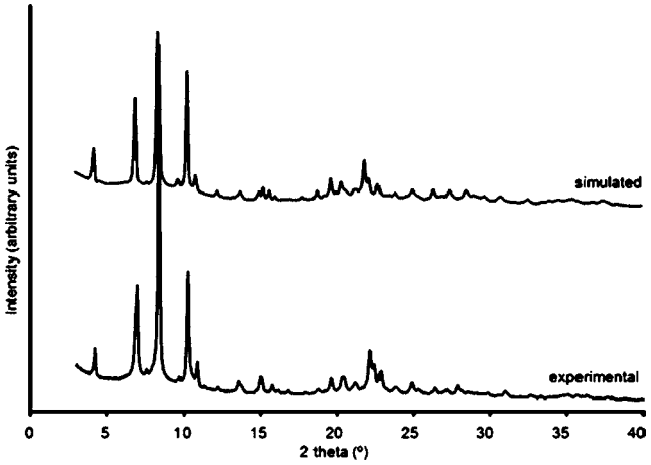

Figure 5. Experimental (bottom) and simulated (top) XRPD patterns of calcined ITQ-38.

The structure of ITQ-38 is related to both ITQ-22 and ITQ-39C, as shown in Figure 4. The relation between ITQ-38 and ITQ-22 is easily seen by comparing the [010] projection of ITQ-38 (Figure 4a) with the [001] projection of ITQ-22 (Figure 4d). Both are built from the same building layer (marked in gray) that can be connected in two different ways. In ITQ-38, adjacent building layers are oriented in the same way and connected to form alternating 6- and 10-rings between the layers (see Figure 4a). In ITQ-22, adjacent layers are related by a b-glide plane perpendicular to the *a*-axis and connected to form 8-rings between the layers (see Figure 4b). The two different possibilities to connect the layers generate stacking disorders in the crystal of ITQ-38.

The structures ITQ-38 and ITQ-39C are also related. Both of them have 16 unique T atoms in the unit cell and crystallize in space group *P*2/*m*. ITQ-39C contains one T atom with 0.5 occupancy whereas in ITQ-38 all atoms are fully occupied. The [101] projection of ITQ-38 (Figure 4c) is similar to the [100] projection of ITQ-39C (Figure 4f), both contain layers of 10-ring channels separated by layers of 4- and 6-rings (in the sequence 6, 6, 4, 6, 6, 4). In contrast, when both structures are viewed along the [010] direction (Figure 4a,e), they look different. ITQ-38 contains alternating 10- and 12-ring channels (Figure 4a), whereas ITQ-39 has twin 12-ring channels (Figure 4e). The two structures have a common building unit (as shown in green in Figure 6), which has the same topology but is slightly distorted in the two structures because of the different connectivity to the neighboring units. The building units are connected via different connecting units (shown in yellow in Figure 6c) to form the 3D frameworks (Figure 6c).

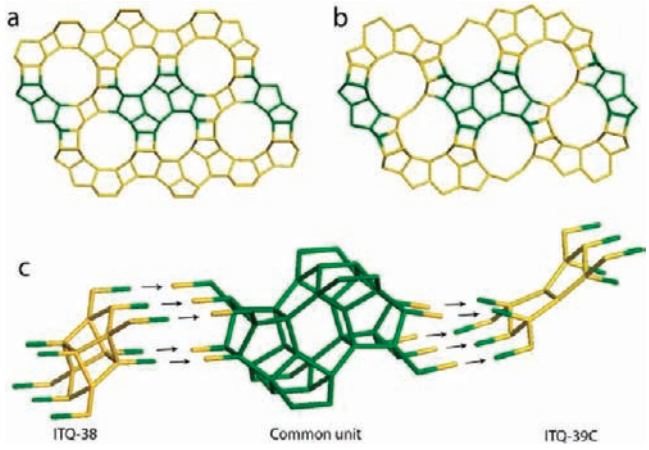

Figure 6. The structure of ITQ-38 (a) and ITQ-39C (b) viewed along the [010] direction with the common building unit marked in green. The common building unit in (c) is further connected via different connecting units (shown in yellow) to form ITQ-38 (left) and ITQ-39C (right), respectively.

The framework density of ITQ-38 is 16.05 T-atom/1000 Å^3, agreeing well with the experimental data (15.9 T-atom/1000 Å^3) and similar to those of ITQ-22 (16.14 T atoms/1000 Å^3) and ITQ-39C (16.06 T-atom/1000 Å^3).

4. CONCLUSIONS

By rationalization of the synthesis procedure, it has been possible to direct the synthesis of a new zeolite, ITQ-38, containing large and medium pores in its structure. The structure has been elucidated by transmission electron microscopy, revealing the presence of very small intergrowth domains with ITQ-22 zeolite. This new material is highly related to ITQ-22 (IWW) and the recently described polymorph C of ITQ-39 (ITQ-39C). ITQ-38 and ITQ-22 are built from the same building layer with different connections. ITQ-39C is only present in 10% enrichment in the ITQ-39 intergrowth zeolite. The structures of ITQ-38 and ITQ-39C have the same 10-ring projection (along [101] of ITQ-38 and [100] of ITQ-39C), and both contain the same building unit. The optimization of the synthesis conditions of ITQ-38, together with rational studies of dicationic piperidine derivative molecules as OSDAs, is a current subject of interest on our group.

■ ASSOCIATED CONTENT

Ⓢ Supporting Information

Synthesis conditions of the zeolite, characterization by X-ray diffraction, thermal and textural analysis, scanning electron microscopy, SAED patterns and atomic coordinates of ITQ-38. This material is available free of charge via the Internet at http://pubs.acs.org.

■ AUTHOR INFORMATION

Corresponding Author

acorma@itq.upv.es; xzou@mmk.su.se.

Notes

The authors declare no competing financial interest.

■ ACKNOWLEDGMENTS

Financial support by the Spanish MICINN (MAT2009-14528-C02-01 and MAT2006-14274-C02-01), Consolider Ingenio

2010-Multicat, Generalitat Valenciana by the PROMETEO program, UPV through PAID-06-11 (n.1952), the Swedish Research Council (VR), the Swedish Governmental Agency for Innovation Systems (VINNOVA) and Göran Gustafsson Foundtion for Natural Sciences and Medical Research, is acknowledged. Manuel Moliner also acknowledges the "Subprograma Ramon y Cajal" for the contract RYC-2011-08972. Wei Wan was supported by a postdoctoral grant from the Carl-Trygger Foundation. The EM facility was supported by Knut and Alice Wallenberg Foundation. The authors thank the beamline BM01B at ESRF in Grenoble for beamtime allocation (exp. CH-2493). Gunnel Karlsson is kindly thanked for TEM sample preparation by ultramicrotomy. Dedicated to Prof. Miguel A. Miranda on his 60th Birthday.

REFERENCES

(1) International Zeolite Association Home Page. http://www.iza-online.org/.
(2) Davis, M. E. *Nature* **2002**, *417*, 813.
(3) (a) Corma, A. *Chem. Rev.* **1997**, *97*, 2373. (b) Auerbach, S. M., Carrado, K. A. Dutta, P. K. ,Eds.; *Handbook of Zeolite Science and Technology*l Marcel Dekker: New York, 2004.
(4) (a) Clark, L. A.; Ye, G. T.; Snurr, R. Q. *Phys. Rev. Lett.* **2000**, *84*, 2893. (b) Kärger, J.; Ruthven, D. M. *Diffusion in Zeolites and Other Microporous Solids*; Wiley: New York, 1992.
(5) (a) Paillaud, J. L.; Harbuzaru, B.; Patarin, J.; Bats, N. *Science* **2004**, *304*, 990. (b) Corma, A.; Diaz-Cabanas, M. J.; Rey, F.; Nicolopoulus, S.; Boulahya, K. *Chem. Commun.* **2004**, *12*, 1356.
(6) Corma, A.; Diaz-Cabañas, M. J.; Jorda, J. L.; Martinez, C.; Moliner, M. *Nature* **2006**, *443*, 842.
(7) (a) Lobo, R. F.; Pan, M.; Chan, I.; Li, H.; Medrud, R. C.; Zones, S. I.; Crozier, P. A.; Davis, M. E. *Science* **1993**, *262*, 1543. (b) Dorset, D. L.; Weston, S. C.; Dhingra, S. S. *J. Phys. Chem. B* **2006**, *110*, 2045. (c) Lobo, R. F.; Davis, M. E. *J. Am. Chem. Soc.* **1995**, *117*, 3766. (d) Corma, A.; Rey, F.; Valencia, S.; Jordá, J. L.; Rius, J. *Nat. Mater.* **2003**, *2*, 493. (e) Simancas, R.; Dari, D.; Velamazán, N.; Navarro, M. T.; Cantín, A.; Jordá, J. L.; Sastre, G.; Corma, A.; Rey, F. *Science* **2010**, *330*, 1219.
(8) Willhammar, T.; Sun, J.; Wan, W; Olevnikov, P.; Zhang, D.; Zou, X.; Moliner, M.; Gonzalez, J.; Martínez, C; Rey, F.; Corma, A. *Nat. Chem.* **2012**, *4*, 188.
(9) Moliner, M.; González, J.; Portilla, M. T.; Willhammar, T.; Rey, F.; Llopis, F. J.; Zou, X. D.; Corma, A. *J. Am. Chem. Soc.* **2011**, *133*, 9497.
(10) (a) O'Keefe, M.; Yaghi, O. M. *Chem.—Eur. J.* **1999**, *5*, 2796. (b) Villaescusa, L. A.; Lighfoot, P.; Morris, R. E. *Chem. Commun.* **2002**, *19*, 2220. (c) Blasco, T.; Corma, A.; Díaz-Cabañas, M. J.; Rey, F.; Vidal-Moya, J. A.; Zicovich-Wilson, C. M. *J. Phys. Chem. B* **2002**, *106*, 2637. (d) Sun, J; Bonneau, C.; Cantín, A; Corma, A.; Diaz-Cabañas, M. J.; Moliner, M.; Zhang, D.; Li, M.; Zou, X. D. *Nature* **2009**, *458*, 1154. (e) Tang, L. Q.; Shi, L.; Bonneau, C.; Sun, J. L.; Yue, H.-J.; Ojuva, A.; Lee, B. L.; Kritikos, M.; Zoltán, B.; Mink, J.; Bell, R. G.; Zou, X. D. *Nat. Mater.* **2008**, *7*, 381.
(11) Newsam, J. M.; Treacy, M. M. J.; Koetsier, W. T.; de Gruyter, C. B. *Proc. R. Soc. London, Ser. A* **1988**, *420*, 375.
(12) Lobo, R. F.; Pan, M.; Chan, I.; Medrud, R. C.; Zones, S. I.; Crozier, P. A.; Davis, M. E. *J. Phys. Chem.* **1994**, *98*, 12040.
(13) (a) Corma, A.; Navarro, M. T.; Rey, F.; Rius, J.; Valencia, S. *Angew. Chem., Int. Ed.* **2001**, *40*, 2277. (b) Conradsson, T.; Dadachov, M. S.; Zou, X. D. *Microporous Mesoporous Mater.* **2000**, *41*, 183. (c) Castaneda, R.; Corma, A.; Fornes, V.; Rey, F.; Rius, J. *J. Am. Chem. Soc.* **2003**, *125*, 7820.
(14) DigitalMicrograph database, www.felmi-zfe.tugraz.at/dm_scripts/.
(15) Wan, W.; Hovmöller, S.; Zou, X. D. *Ultramicroscopy* **2012**, *115*, 50.
(16) Wan, W. CrystDiffract. http://www.mmk.su.se/electron-crystallography.
(17) Hovmöller, S. *Ultramicroscopy* **1992**, *41*, 121−135.
(18) Corma, A.; Davis, M. E. *Chem. Phys. Chem.* **2004**, *5*, 304.
(19) (a) Kessler, H. *Mater. Res. Soc. Symp. Proc.* **1991**, *233*, 47. (b) Barret, P. A.; Camblor, M. A.; Corma., A.; Jones, R. H.; Villaescusa, L. A. *J. Phys. Chem. B* **1998**, *102*, 4147. (c) Zones, S. I.; Burton, A. W.; Lee, G. S.; Olmstead, M. M. *J. Am. Chem. Soc.* **2007**, *129*, 9066. (d) Cantin, A.; Corma, A.; Díaz-Cabañas, M. J.; Jorda, J. L.; Moliner, M.; Rey, F. *Angew. Chem., Int. Ed.* **2006**, *45*, 8013. (e) Cantin, A.; Corma, A.; Diaz-Cabanas, M. J.; Jorda, J. L.; Moliner, M. *J. Am. Chem. Soc.* **2006**, *128*, 4216.
(20) Koller, H.; Wolker, A.; Eckert, H.; Panz, C.; Behrens, P. *Angew. Chem., Int. Ed. Engl.* **1997**, *36*, 2823.
(21) Zones, S. I.; Hwang, S.-J.; Elomari, S.; Ogino, I.; Davis, M. E.; Burton, A. W. *C. R. Chim.* **2005**, *8*, 267.
(22) Zones, S. I.; Hwang, S.-J. *Microporous Mesoporous Mater.* **2003**, *58*, 263.
(23) Werner, P. E.; Eriksson, L.; Westdahl, M. J. *Appl. Crystallogr.* **1985**, *18*, 367.
(24) (a) DeRosier, D. J.; Klug, A. *Nature* **1968**, *217*, 130. (b) Hovmöller, S.; Sjögren, A.; Farrants, G.; Sundberg, M.; Marinder, B. O. *Nature* **1984**, *311*, 238.
(25) (a) Gramm, F.; Baerlocher, Ch.; McCusker, L. B.; Warrender, S. J.; Wright, P. A.; Han, B.; Hong, S. B.; Liu, Z.; Ohsuna, T.; Terasaki, O. *Nature* **2006**, *444*, 79. (b) Baerlocher, C.; Gramm, F.; Massüger, L.; McCusker, L. B.; He, Z.; Hovmöller, S.; Zou, X. *Science* **2007**, *315*, 1113. (c) Baerlocher, Ch.; Xie, D.; McCusker, L. B.; Hwang, S.-J.; Chan, I. Y.; Ong, K.; Burton, A. W.; Zones, S. I. *Nat. Mater.* **2008**, *7*, 631. (d) Jiang, J.-X.; Jordá, J. L.; Yu, J.; Baumes, L. A.; Mugnaioli, E.; Diaz-Cabañas, M. J.; Kolb, U.; Corma, A. *Science* **2011**, *333*, 1331. (e) Sun, J.; He, Z.; Hovmöller, S.; Zou, X.; Gramm, F.; Baerlocher, Ch; McCusker, L. B. *Z. Kristallogr.* **2010**, *225*, 77.
(26) Rodriguez-Carvajal, J. *Comm. Powder Diffr. (IUCr) Newslett.* **2001**, *26*, 12.